J Appl Electrochem (2010) 40:575–580
DOI 10.1007/s10800-009-0032-y

ORIGINAL PAPER

Direct-hydrothermal synthesis of $LiFe_{1-x}Mn_xPO_4$ cathode materials

Jing Xu · Gang Chen · Hong-Jian Li · Zu-Shui Lv

Received: 4 April 2009 / Accepted: 23 November 2009 / Published online: 5 December 2009

Abstract Carbon free $LiFe_{1-x}Mn_xPO_4$ ($x = 0$, 0.05, 0.1, 0.2, 0.4) cathode materials were prepared by a direct-hydrothermal process at 170 °C for 10 h. The structural and electrochemical properties of the samples were characterized by X-ray diffraction (XRD), scanning electron microscopy (SEM), charge–discharge experiments, cyclic voltammetry (CV) and alternating current (AC) impedance spectroscopy. The electrochemical performance of $LiFePO_4$ prepared in this manner showed to be positively affected by Mn^{2+}-substitution. Among the Mn^{2+}-substitution samples, the $LiFe_{0.9}Mn_{0.1}PO_4$ exhibited an initial discharge capacity of 141.4 mA h g^{-1} at 0.1 C, and the capacity fading is only 2.7% after 50 cycles.

Keywords $LiFePO_4$ · Hydrothermal process · Mn^{2+} substitution

1 Introduction

First proposed by Padhi et al. [1], $LiFePO_4$ has become a very attractive cathode material for lithium-ion batteries due to its high theoretical capacity (170 mA h g^{-1}) [2], high potential (3.4 V vs. Li/Li^+) [3], cheapness, low toxicity [4], and excellent thermal stability [5, 6]. However the low electronic conductivity and lithium-ion diffusivity limit its commercial applications. Improvements in conductivity have been achieved by carbon coating [7] or metal ions doping [8, 9]. The way to solve the limitation of lithium-ion diffusion focuses mainly on particle size reduction [3]. Although carbon coating is a common way to enhance the electronic conductivity, it not only leads to a loss in energy density but also helps nothing in the intrinsic electronic conductivity or chemical diffusion coefficient of lithium within the crystal [10]. Metal ions doping was a feasible way to enhance the intrinsic conductivity such as the Li-site doping with Mg, Ti, Zr, Cr, Nb and Mo [8, 11–15]. The Fe-site doping could weaken the Li–O interaction, resulting in high ionic mobility and diffusion coefficient [16–20]. Recent researches have suggested that V, Ni, Co, Mg, Zn, Al and Mn substitution of Fe can improve the electrochemical behavior of $LiFePO_4$ by increasing the intrinsic electronic conductivity [21–24]. For example, Tatsuya Nakamura et al. have proposed that Mn^{2+}-substitution of partial Fe^{2+} could enhance the bulk conductivity [25].

More recently, hydrothermal synthesis has been chosen to prepare $LiFePO_4$ for its advantages: simple synthesis process and low energy consumption [26–32]. But all those have low capacity, or require a high temperature firing after hydrothermal process, or need to induce conducting phase coating on $LiFePO_4$ particles in order to obtain high capacity. However, there are few reports on hydrothermal synthesis of $LiFePO_4$ with Mn^{2+}-substitution (actually concerning the effect of Mn^{2+} on the electrochemical properties of $LiFePO_4$ prepared via hydrothermal route).

Therefore, a series of carbon free $LiFe_{1-x}Mn_xPO_4$ ($x = 0$, 0.05, 0.1, 0.2, 0.4) cathode materials were synthesized with a direct-hydrothermal method, which did not require a high temperature firing after hydrothermal process and facilitated practical application. The electrochemical properties of the synthesized powders were discussed in this work and the emphasis of the current

J. Xu · G. Chen (✉) · H.-J. Li · Z.-S. Lv
Department of Applied Chemistry, Harbin Institute of Technology, 150001 Harbin, Peoples Republic of China
e-mail: gchen@hit.edu.cn

investigation was to study the effect of Mn^{2+}-substitution on capacity retention and cycle stability.

2 Experimental

$LiFe_{1-x}Mn_xPO_4$ ($x = 0$, 0.05, 0.1, 0.2, 0.4) was prepared by a direct-hydrothermal process from $LiOH{\cdot}H_2O$, $FeSO_4{\cdot}7H_2O$, H_3PO_4, and $MnSO_4{\cdot}H_2O$. After $LiOH{\cdot}H_2O$ was dissolved in distilled water to obtain 1 M solution, H_3PO_4, $FeSO_4{\cdot}7H_2O$ and $MnSO_4{\cdot}H_2O$ powders were added to LiOH solution in a molar ratio for Li:Fe:P:Mn = 3:1 − x:1:x ($x = 0$, 0.05, 0.1, 0.2, 0.4). In order to prohibit the conversion of Fe^{2+} to Fe^{3+}, the mixing process was carried out under Ar atmosphere. The precursor solution of 50 mL was put into a stainless steel autoclave, and the reactor was heated at 170 °C for 10 h. The final solution was cooled and filtered. Then the obtained precipitates were dried at 100 °C for 2 h in a vacuum oven.

The crystalline phases were identified on a D/MAX-RC X-ray diffraction (XRD, Rigaku) using Cu K_α radiation ($\lambda = 1.5418$ Å). The 2θ Bragg angles were scanned over a range of 10–80° with a step size of 0.02°. The morphology of particle was observed with a scanning electron microscope (SEM, S-4700, Hitachi). The XPS spectra were collected on an American Electronics physical PHI5700ESCA system X-ray photoelectron spectroscope using AlK radiation. The source was operated at 12.5 kV and the anode power was 250 W. The banding energy (BE) was calibrated with the C1s peak.

The electrodes were prepared by spreading the cathode slurry (75 wt% of the active material, 10 wt% of polyvinylidene fluoride (PVDF) in *N*-methyl pyrrolidone (NMP), and 15 wt% of carbon black) onto an aluminum foil followed by drying in vacuum at 120 °C for 12 h. The cathode thickness reached approximately 0.1 mm, and its surface area is about 1.77 cm^{-2}. The loading of the active materials is about 1.69–1.27 mg cm^{-2}. The cells (CR2025) were assembled in an argon filled glove-box using lithium metal foil as the counter electrode. The electrolyte was 1.0 mol dm^{-3} $LiPF_6$ in a mixture of ethylene carbonate (EC) and dimethyl carbonate (DEC) (1:1, v/v).

The cells were galvanostatically charged and discharged over a voltage range of 2.5–4.5 V at different rates. The C rate was calculated from the weight and theoretical capacity of $LiFePO_4$ (1C = 170 mA h g^{-1}). Electrochemical impedance spectroscopy (EIS) and cyclic voltammetry (CV) were measured on an electrochemical workstation (CHI 604C). CV was carried out at a scanning rate of 0.1 mV s^{-1} between 2.5 and 4.5 V (vs. Li/Li^+). EIS measurements were performed over a frequency range of 100 kHz–10 mHz at a charged stage with an applied amplitude of 5 mV.

3 Results and discussion

3.1 Crystalline structure analysis

Figure 1 shows the X-ray diffraction patterns of the $LiFe_{1-x}Mn_xPO_4$ ($x = 0$, 0.05, 0.1, 0.2, 0.4) compounds. All samples exhibit single phase of $LiFePO_4$ with an ordered olivine structure indexed to the orthorhombic *Pnma* space group. The FWHM of the diffraction peaks descend after substitution, this demonstrates Mn^{2+}-substitution intensity the crystallinity of $LiFePO_4$. The change of the unit cell volume as a function of x in $LiMn_xFe_{1-x}PO_4$ is presented in Fig. 2. As the ionic size of Mn^{2+} (0.08 nm) [33] is larger than that of Fe^{2+} (0.078 nm) [34], as x increases, the unit cell volume increases linearly with Mn^{2+}-substitution according to Vegard's law which is consistent with the literature reported [35, 36]. These indicate that Mn^{2+} was

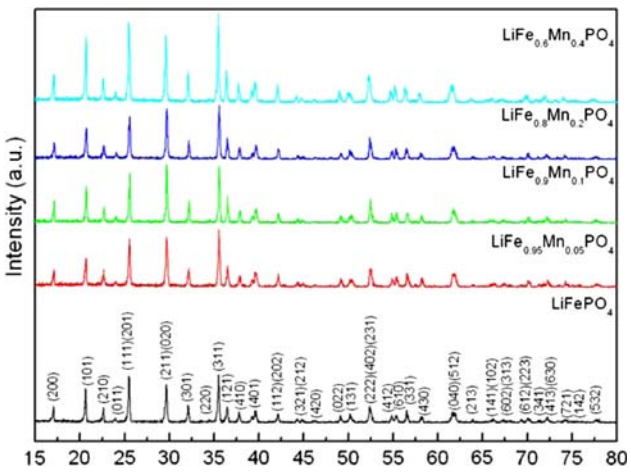

Fig. 1 XRD patterns of $LiFe_{1-x}Mn_xPO_4$ ($x = 0$, 0.05, 0.1, 0.2, 0.4) compounds

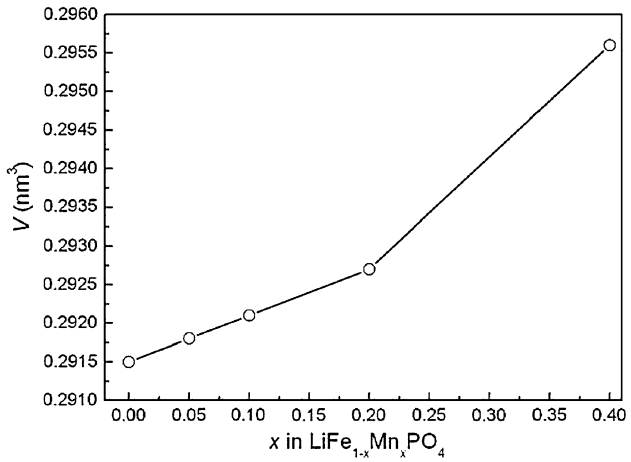

Fig. 2 Variation of unit cell volume as a function of Mn contents in $LiFe_{1-x}Mn_xPO_4$

successfully introduced into $LiFePO_4$ matrix structure and the incorporation of Mn^{2+} did not alter the $LiFePO_4$ structure but slightly increased unit cell volume. The extension in the unit cell volume could facilitate the intercalation and deintercalation of lithium.

XPS analysis is performed to investigate the chemical composition and valent states of the $LiFe_{1-x}Mn_xPO_4$ ($x = 0, 0.1$) samples. Figure 3a shows the peaks at 710.5, 531.0 and 131.1 eV which are due to Fe2p, O1s and P2p in $LiFe_{1-x}Mn_xPO_4$ ($x = 0, 0.1$) samples respectively. Figure 3b presents Mn2p XPS spectra in $LiFe_{0.9}Mn_{0.1}PO_4$ and it could be found the banding energy (BE) of $Mn2p_{3/2}$ peak at 640.7 eV is typical for Mn^{2+} state [33]. The $Fe2p_{3/2}$ peak with a BE of 710.0 eV of $LiFePO_4$ corresponds to Fe^{2+} state [36], and no shift is found for $LiFe_{0.9}Mn_{0.1}PO_4$ which indicated the Mn^{2+}-substitution has no influence on the Fe^{2+} state [37]. However, as Xie and Zhou reported [10], Li1s emission is not seen clearly because it is superposed on the Fe3p peak at about 56 eV. The XPS results showed that the oxidation states of Fe and Mn in the compounds are 2 and to a rough approximation, the Fe:Mn:P molar ratio is about 0.9:0.1:1, which is equal to the expectable value.

3.2 Microstructure of the powders

The effects of Mn^{2+}-substitution on the particles size and morphology of $LiFePO_4$ have been investigated by SEM. Figure 4 shows the SEM images of the $LiFe_{1-x}Mn_xPO_4$ compounds with various Mn^{2+} contents. All prepared samples are composed of platelet particles with size of approximate $0.5 \times 0.5 \times 2\ \mu m^3$ and the particle size of $LiFe_{1-x}Mn_xPO_4$ ($x \leq 0.2$) decreases as Mn^{2+} content increasing. When x increases to 0.2 and 0.4, the morphology of the sample shows slightly particle-agglomerated.

3.3 Electrochemical performance

Cyclic voltammetry is performed in order to investigate the effect of Mn^{2+}-substitution on the electrochemical properties of $LiFePO_4$ by using a scanning rate of 0.1 mV s^{-1}. The CV profiles of $LiFe_{1-x}Mn_xPO_4$ are shown in Fig. 5. They both exhibit a pair of redox peaks around 3.4 V vs. Li/Li^+, but they vary the intensities of the peaks. The peak value increased with the substitution degree up to 0.1, took a maximum and then decreased with further increase in the substitution. But they are much higher than that of

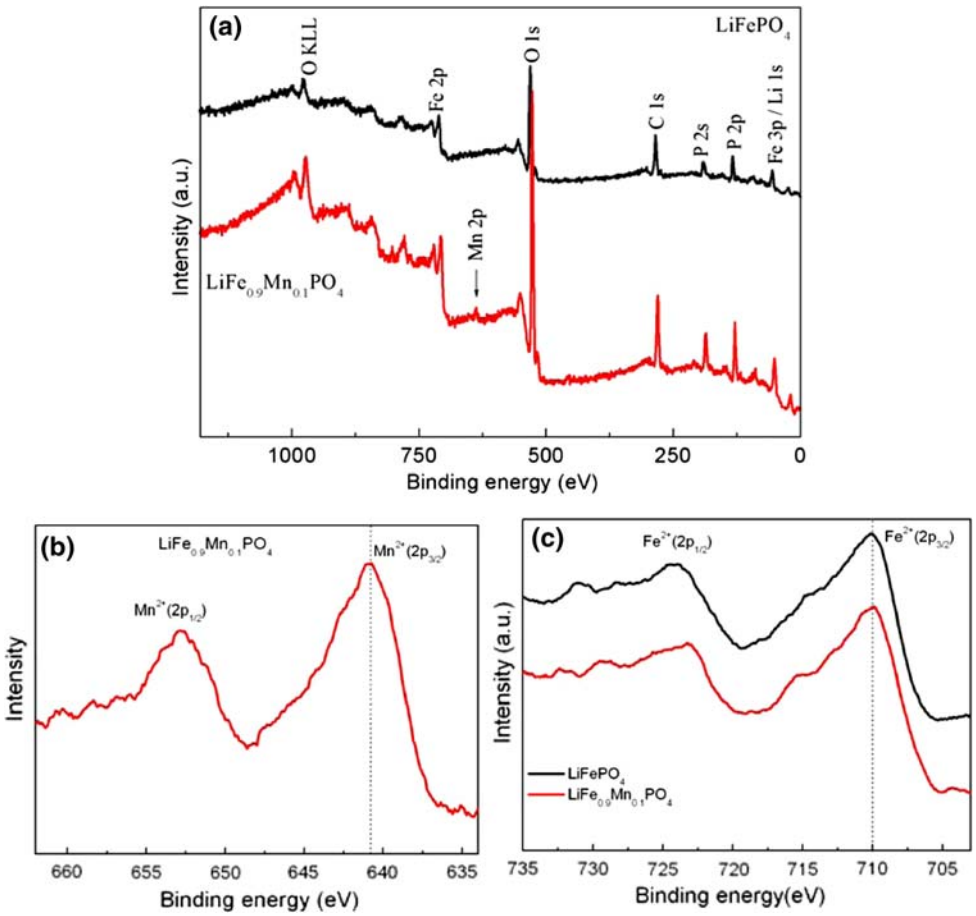

Fig. 3 XPS spectra **a** of $LiFe_{0.9}Mn_{0.1}PO_4$ and $LiFePO_4$ samples, **b** for Mn2p in $LiFe_{0.9}Mn_{0.1}PO_4$, **c** for Fe2p in $LiFe_{0.9}Mn_{0.1}PO_4$ and $LiFePO_4$

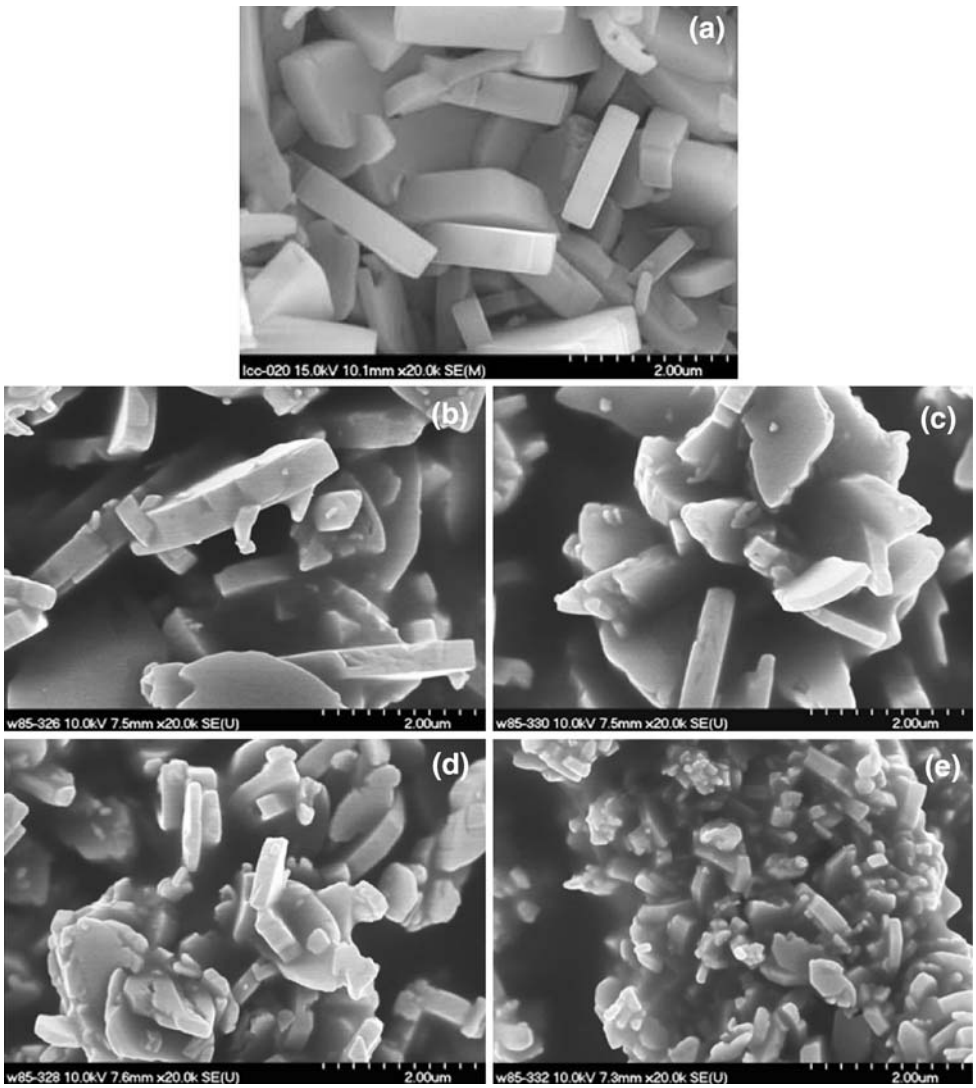

Fig. 4 SEM images of $LiFe_{1-x}Mn_xPO_4$ compounds **a** $x = 0$, **b** $x = 0.05$, **c** $x = 0.1$, **d** $x = 0.2$, **e** $x = 0.4$

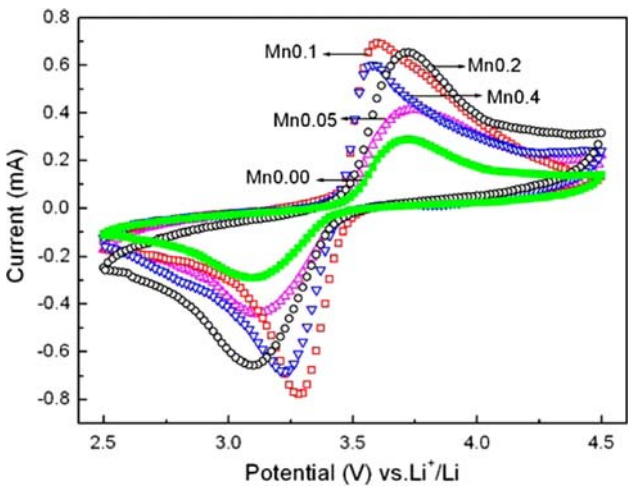

Fig. 5 Cyclic voltammetry profiles of $LiFe_{1-x}Mn_xPO_4$

$LiFePO_4$, indicating the higher electrochemical reactivity of Mn^{2+}-substitution electrodes.

It was thought that the Mn^{2+}-substitution had no direct contribution to the electrochemical reaction but enhanced both electronic and ionic conductivities [25]. So the electrochemical delithiation/lithiation mechanism of $LiFe_{0.9}Mn_{0.1}PO_4$ electrode could be written as:

$$\text{Charge: } LiFePO_{4-x} - Li^+ - xe- \rightarrow xFePO_4 + (1-x)LiFePO_4$$

$$\text{Discharge: } FePO_4 + xLi^+ + xe- \rightarrow xLiFePO_4 + (1-x)FePO_4$$

Figure 6 shows the initial charge–discharge curves of $LiFe_{1-x}Mn_xPO_4$ at 0.1 C. All the samples have similar charge–discharge curves with flat plateaus corresponding to the lithium delithiation/lithiation reactions but they vary in

plateau voltages. The result indicates a decrease in polarization of substitution electrode during cycling. Among the $LiFe_{1-x}Mn_xPO_4$ samples, $LiFe_{0.9}Mn_{0.1}PO_4$ exhibited the highest discharge capacity of 141.4 mA h g^{-1}, about 83% of the theoretical capacity of $LiFePO_4$. But the discharge capacity decreased with further increase Mn^{2+}-substitution degree. It is possible to explain the experimental facts from the viewpoint of that in Mn-rich phase the lattice frustration during delithiation–lithiation process induced by the strong electron Mn^{3+}/Mn^{2+} Jahn–Teller effect, Li^+ couldn't migrate reversibly [1, 25]. Additionally, the peak separation corresponded to the polarization degree increased with further increase in the substitution which is consistent with the literature reported [25].

The cycle life of all the samples at 0.1 C rate to a cut-off voltage between 2.5 and 4.5 V is shown in Fig. 7. For $LiFePO_4$ and $LiFe_{0.6}Mn_{0.4}PO_4$, the initial discharge capacity decreases rapidly from 91.4 and 77.1 mA h g^{-1} to 65.4 and 67.2 mA h g^{-1} at 50th cycle, showing the poorest cycle performance. However, the samples of $LiFe_{1-x}Mn_xPO_4$ with $x = 0.05$, 0.1, 0.2 show much better cycling performance. The capacity fading of $LiFe_{0.9}Mn_{0.1}PO_4$ is only 2.7% after 50 cycles.

The electronic conductivities of prepared samples are measured with the four-electrode method. The measurements are performed in the air at room temperature, and the data was listed in Table 1. $LiFe_{0.9}Mn_{0.1}PO_4$ shows the highest electronic conductivity among all samples, which is almost 2 orders of magnitude higher than that of pure sample. The highest conductivity of $LiFe_{0.9}Mn_{0.1}PO_4$ may be attributed to the uniformly distributed smaller size of particle, since the particles with smaller size will provide more contacts between particles [38]. On the other hand, Mn^{2+}-substitution could decrease the band gap of $LiFePO_4$ [39] which plays a positive effect on improved conductivity of $LiFePO_4$.

To provide more information for the improved electrochemical properties, AC impedance measurements are performed on all the samples at the charged state after 5 cycling (Fig. 8). It is composed of a depressed semicircle in the moderate frequency region and a spike in the low frequency region. The semicircle is related to the charge-transfer resistance (R_{ct}), and the spike is attributed to the Warburg impedance of long-range Li-ion diffusion [40]. Comparing the semicircles of the pristine and substitution

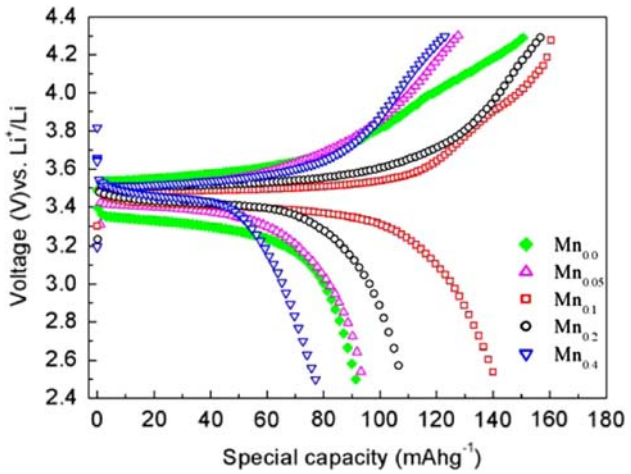

Fig. 6 Charge–discharge curves of $LiFe_{1-x}Mn_xPO_4$

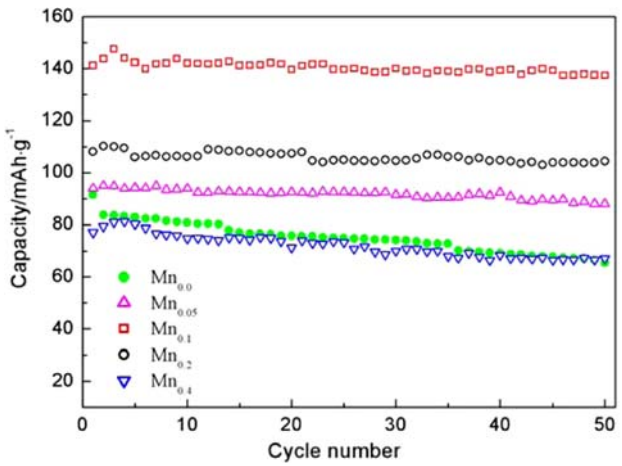

Fig. 7 Cycling performance of $LiFe_{1-x}Mn_xPO_4$ at 0.1 °C

Table 1 Electronic conductivity of prepared samples

	κ (S cm^{-1})
$LiFePO_4$	2.1×10^{-9}
$LiFe_{0.95}Mn_{0.05}PO_4$	9.6×10^{-8}
$LiFe_{0.9}Mn_{0.1}PO_4$	1.9×10^{-7}
$LiFe_{0.8}Mn_{0.2}PO_4$	1.6×10^{-7}
$LiFe_{0.6}Mn_{0.4}PO_4$	1.1×10^{-7}

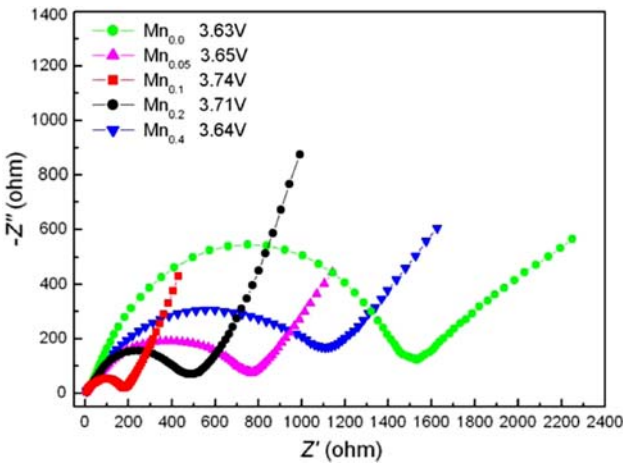

Fig. 8 Nyquist plots of $LiFe_{1-x}Mn_xPO_4$

samples in the moderate frequency region, it is evident that the R_{ct} was decreased by Mn^{2+}-substitution which facilitating kinetics of electrochemical reactions, further leading to better electrochemical performances [40]. Among all the samples, $LiFe_{0.9}Mn_{0.1}PO_4$ exhibited the lowest R_{ct}, which is also confirmed from the flatter charge–discharge plateaus for the $LiFe_{0.9}Mn_{0.1}PO_4$ electrode.

The Mn^{2+}-substitution provides the influences on both the interface and bulk properties of $LiFePO_4$ such as downsizing of the particles and enhancement of the bulk electronic conductivity. It results in the improvement of the electrochemical performance of $LiFePO_4$, such as the initial capacity, the capacity retention and the polarization degree. However, it is difficult to discuss their contributions quantitatively and separately, the further study is under work in our laboratory.

4 Conclusions

In this study, the carbon free $LiFe_{1-x}Mn_xPO_4$ ($x = 0$, 0.05, 0.1, 0.2, 0.4) materials were successfully synthesized via a direct-hydrothermal method. X-ray diffraction analyses indicate that Mn^{2+}-substitution did not alter the crystal structure of $LiFePO_4$ phase. It was found that the Mn^{2+}-substitution had some influences on the electrochemical performance of the olivine cathode: the enhancement of the initial capacity, the suppression of the cycle fading, and the lowering of polarization. They were attributed partly to the decrease of the charge-transfer resistance. In particular, the carbon free $LiFe_{0.9}Mn_{0.1}PO_4$ exhibited a specific capacity of 141.4 mA h g^{-1} at 0.1 C, and also showed obviously better cycling life than the other samples.

Acknowledgments This work was supported by National Science Foundation of China (Project No.20571019) and SRF for ROCS, HLJ (LC06C13).

References

1. Padhi A, Nanjundaswamy K, Goodenough J (1997) J Electrochem Soc 144:1188
2. Padhi A, Nanjundaswamy K, Okada S, Goodenough J (1997) J Electrochem Soc 144:1609
3. Yamada A, Chung SC, Hinokuma K (2001) J Electrochem Soc 148:A224
4. Wu YP, Dai XB, Ma JQ, Chen YJ (2004) Lithium ion batteries: practice and application. Chemical Industry Press, Beijing
5. MacNeil DD, Lu ZH, Chen ZH, Dahn JR (2002) J Power Sources 108:8
6. Takahashi M, Tobishima S, Takei K, Sakurai Y (2002) Solid State Ion 148:283
7. Huang H, Yin SC, Nazar LF (2001) Electrochem Solid-State Lett 4:A170
8. Chung SY, Bloking JT, Chiang YM (2002) Nat Mater 1:123
9. Park KS, Son JT, Chung HT, Kim SJ, Lee CH, Kang KT, Kim HG (2004) Solid State Commun 129:311
10. Xie H, Zhou ZT (2006) Electrochim Acta 51:2063
11. Gouveia DX, Lemos V, de Paiva JAC, Souza Filho AG, Mendes Filho J, Lala SM, Montoro LA, Rosolen JM (2005) Phys Rev B 72:24105
12. Striebel K, Guerfi A, Shim J (2003) J Power Sources 119–121:951
13. Ying J, Lei M, Jiang C (2003) J Power Sources 158:547
14. Wang GX, Needham S, Yao J (2006) J Power Sources 159:284
15. Delacourt C, Wurm C, Laffont L (2006) Solid State Ion 177:340
16. Zhang M, Jiao L-F, Yuan H-T (2006) Solid-State Ion 177:3309
17. Abbate M, Lala SM, Montoro LA, Rosolenb JM (2005) Electrochem Solid State Lett 8(6):A288
18. Wang D, Li H, Shi S, Huang X, Chen L (2005) Electrochim Acta 50:2958
19. Prosini PP, Zane D, Pasquali M (2001) Electrochim Acta 46:3517
20. Baker J, Saidi MY, Swoyer JL (2003) Electrochem Solid State Lett 6:A53
21. Wen Y, Zeng L, Tong Z (2006) J Alloys Compd 416:208
22. Liu H, Cao Q, Fu LJ (2006) Electrochem Commun 8:1553
23. Nakamura T, Miwa Y, Tabuchi M, Yamada Y (2006) J Electrochem Soc 153:A1108
24. Shanmukaraj D, Wang GX, Muruganc R, Liu HK (2008) Mater Sci Eng B 149:93–98
25. Nakamura T, Sakumoto K, Okamoto M (2007) J Power Sources 435-441:174
26. Lee J, Teja AS (2006) Mater Lett 60:2105
27. Dokko K, Koizumi S, Sharaishi K, Kanamura K (2007) J Power Sources 165:656
28. Meligrana G, Gerbaldi C, Tuel A, Bodoardo S, Penazzi N (2006) J Power Sources 160:516
29. Chen J, Whittingham MS (2006) Electrochem Commun 8:855
30. Tajimi S, Ikeda Y, Uematsu K, Toda K, Sato M (2004) Solid State Ion 175:287
31. Franger S, Cras FL, Bourbon C, Rouault H (2003) J Power Sources 119:252
32. Xua C, Lee J, Teja AS (2008) J Supercrit Fluids 44:92–97
33. Cao HT, Pei ZL, Gong J, Sun C, Huang RF, Wen LS (2004) J Solid State Chem 177:1484
34. Saiful Islam M, Driscoll DJ, Fisher CAJ, Slater PR (2005) Chem Mater 17:5088
35. Yamada A, Hosoya M, Chung S-C (2003) J Power Sources 119–121:234
36. Myung S-T, Komaba S, Hirosaki N, Yashiro H, Kumagai N (2004) Electrochim Acta 49:4215
37. Lee CY, Tsai HM, Chuang HJ, Li SY, Lin P, Tseng TY (2005) J Electrochem Soc 152:A716
38. Yang M-R, Ke W, Wu S (2007) J Power Sources 165:647
39. Jing Xu, Chen G Phys B: Condens Matter. Online
40. Liu H, Wang GX, Wexler D, Wang JZ, Liu HK (2008) Electrochem Commun 10(1):165–169